

# FLOL: Fast Baselines for Real-World Low-Light Enhancement

Juan C. Benito<sup>1</sup>, Daniel Feijoo<sup>1</sup>, Alvaro Garcia<sup>1</sup>, Marcos V. Conde<sup>1,2</sup>

<sup>1</sup> Cidaut AI, Spain

<sup>2</sup> Computer Vision Lab, University of Würzburg

<https://github.com/cidautai/FLOL>

## Abstract

*Low-Light Image Enhancement (LLIE) is a key task in computational photography and imaging. The problem of enhancing images captured during night or in dark environments has been well-studied in the image signal processing literature. However, current deep learning-based solutions struggle with efficiency and robustness in real-world scenarios (e.g. scenes with noise, saturated pixels, bad illumination). We propose a lightweight neural network that combines image processing in the frequency and spatial domains. Our method, FLOL+, is one of the fastest models for this task, achieving state-of-the-art results on popular real scenes datasets such as LOL and LSRW. Moreover, we are able to process 1080p images under 12ms. Our code and models will be open-source.*

## 1. Introduction

The performance of imaging systems can be disrupted in low-light conditions. For instance, detection and action recognition algorithms might struggle in conditions of low illumination, under-exposure, extreme noise, and specially at night [34, 50, 56, 57]. Therefore, it is essential in image processing to find a reliable solution that allows to improve exposure and “lighten” dark images correctly.

The image restoration problem [10] for night or dark images could be formulated as:

$$\mathbf{y} = \gamma(\mathbf{x}) + \mathbf{n} \quad (1)$$

where  $\mathbf{y}$  is the captured image,  $\mathbf{x}$  is the underlying clean signal,  $\gamma$  is a function for the response of the camera sensor (e.g. ISO gain, clip saturated pixels), and  $\mathbf{n}$  is the sensor read-shot noise — especially strong during night due to the lack of photon readings by the camera sensor [17]. For simplification, as previous works we will ignore the possible blur effects and other optics-related artifacts such as glare and flare.

Diverse techniques have been proposed to solve this problem *i.e.*, reconstruct  $\mathbf{x}$  from  $\mathbf{y}$ , these are classified into

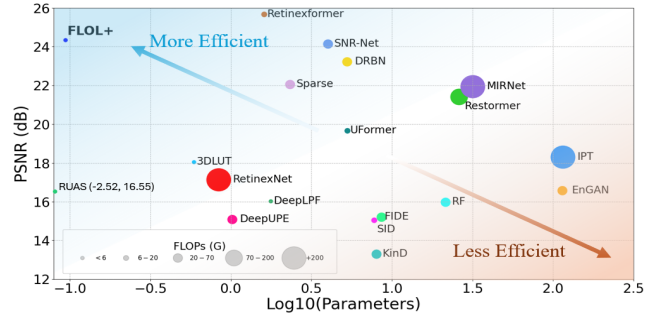


Figure 1. Comparison of model performance on the LOLv2-Synthetic [55] dataset. The chart displays the PSNR value reached for each model depending on its number of parameters, represented here by the decimal logarithm of such number in millions. The size of the points is proportional to the FLOPs of each model. Methods placed in the left-upper corner are more efficient than those placed on the right-lower corner of the chart.

two groups: deep learning-based techniques [11, 21, 40, 46] and classical techniques [23, 25, 64]. Nowadays, deep learning methods are widely considered the state-of-the-art for this task [4, 31].

Most deep learning solutions based on convolutional neural networks (CNNs) require millions of parameters to achieve an acceptable reconstruction performance in terms of PSNR and SSIM [44] (please see Fig. 1). As a result, most methods lack of **efficiency** in terms of memory and runtime *i.e.*, they cannot enhance images in real-time (50ms per image or 20FPS).

Besides efficiency, low-light image enhancement solutions struggle to **generalize** in real scenes (“in the wild”). We find several real and synthetic datasets for this task such as LOLv2 [55], and it is well-known that models trained on synthetic data fail to generalize on real cases [1, 8]. The reason is the domain gap between the simulated conditions and the real-world conditions; most approaches assume  $\mathbf{n}$  to follow a Gaussian distribution, and  $\gamma$  to be a linear function, when in reality the camera sensor’s noise and response is more complex. LLIE models must be robust to out-of-

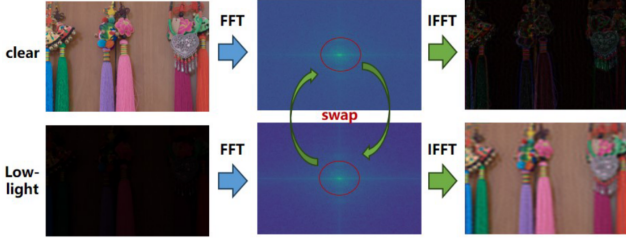


Figure 2. The illumination information is retained in the amplitude component within the Fourier space [27, 40]. Thus, many LLIE methods operate in the frequency domain. Source image from [19].

distribution (OOD) conditions [31]. Therefore, we focus on solving these two problems in LLIE: efficiency and robustness in real scenarios – see Figs. 4, 5 and 6.

Following previous works such as *RetinexNet* [46], *FourLLIE* [40] and *SNR-Net* [51], we study how to build a compact and efficient model using two components or stages: first, a frequency stage, where we estimate and process the amplitude component of the image; second, the (spatial) denoising stage, where the model will focus on improving details and reducing noise. This allows to tackle directly the two degradation components in the inverse problem (Eq. 1): the illumination-related  $\gamma$  and the noise  $\mathbf{n}$ .

Our model is trained on diverse real scenes to improve its robustness on these cases. The 2-stage approach allows us to design compact models for each sub-task, which brings efficiency and certain control or interpretability.

**Our contributions can be summarized as follows:**

- 1) We introduce a new lightweight and fast baseline model for low-light image enhancement (see Fig. 1).
- 2) We achieve state-of-the-art (SOTA) performance on real-world low-light enhancement benchmarks.
- 3) Our method requires  $10\times$  less parameters than others and can process HD images in real-time at 12ms.

## 2. Related Work

### 2.1. Low-Light Image Enhancement

The principal task in LLIE consists in correcting the illumination level of dark and under-exposed images properly, without adding artifacts or noise. Most recent solutions are based on CNNs which are widely used as an end-to-end solution to this problem by implementing effective neural network architectures.

Some methods apply traditional image decomposition like *RetinexNet* [46]. They are capable of reaching higher quality images by estimating illumination and reflectance maps. *Retinexformer* [4] is the most competitive retinex-based method, based on attention-based mechanisms such as the Transformer [38]. Other procedures employ unsuper-

vised learning, focusing on the illumination curves estimation or the improvement of illumination learning to perform a good light correction [14, 31]. Further, *Xu et al.* [51] introduced a method that pays attention to the *Signal-to-Noise-Ratio* (SNR) in the dark (noisy) images. This makes possible to enhance “pixel by pixel” regions with lower SNR associated with dimmer regions of the image.

There are recent models that leverage Fourier information to solve LLIE. For example, *Li et al.* [26] studies how to extract lightness and noise in the Fourier space. They noticed that it is beneficial to incorporate space and frequency information into neural networks. Also, *Huang et al.* [18] suggested before that illumination information is contained within the amplitude component, thus, this component differs from low to high images and it is related to the lightness level on images (please see Fig. 2). In consequence, this property was exploited by *Wang et al.* in *FourLLIE* [40], where they developed a new 2-stage deep neural network to enhance dark images using Fourier frequency information.

### 2.2. Fourier Theory

Fourier information has been proved to be helpful in many computer vision tasks. Firstly, the Fourier theory was considered on hazy images and pan-sharpening methods [59, 65, 66]. Additionally, *Xu et al.* [49] adopted a data augmentation technique based on Fourier frequency information. *Zhou et al.* [67] built a Fourier-based super-resolution method. Another example is *Fuoli et al.* [13], which also presented a special loss based on Fourier theory that attempts to restore high-frequency information in super-resolution problems. Last but not least, *Wang et al.* [40] applied Fourier frequency information to the LLIE problem. They built a new Fourier-based network called *FourLLIE* which includes the phase and amplitude Fourier images along with SNR map introduced by *Xu et al.* [51], this helps to remove noise generated during previous illumination phase.

We further investigate about how to minimize the number of FLOPs and parameters by improving the method introduced in [40] without losing performance. For this reason, the new model will be lighter since it requires less memory, and it will be able to process high-resolution images faster.

## 3. Proposed Method

First of all, given an input image  $x$  of size  $(H, W)$  the discrete Fourier transform can be calculated following the relation below:

$$X(u, v) = \frac{1}{\sqrt{HW}} \sum_{h=0}^{H-1} \sum_{w=0}^{W-1} x(h, w) e^{-i2\pi\left(\frac{h}{H}u + \frac{w}{W}v\right)} \quad (2)$$

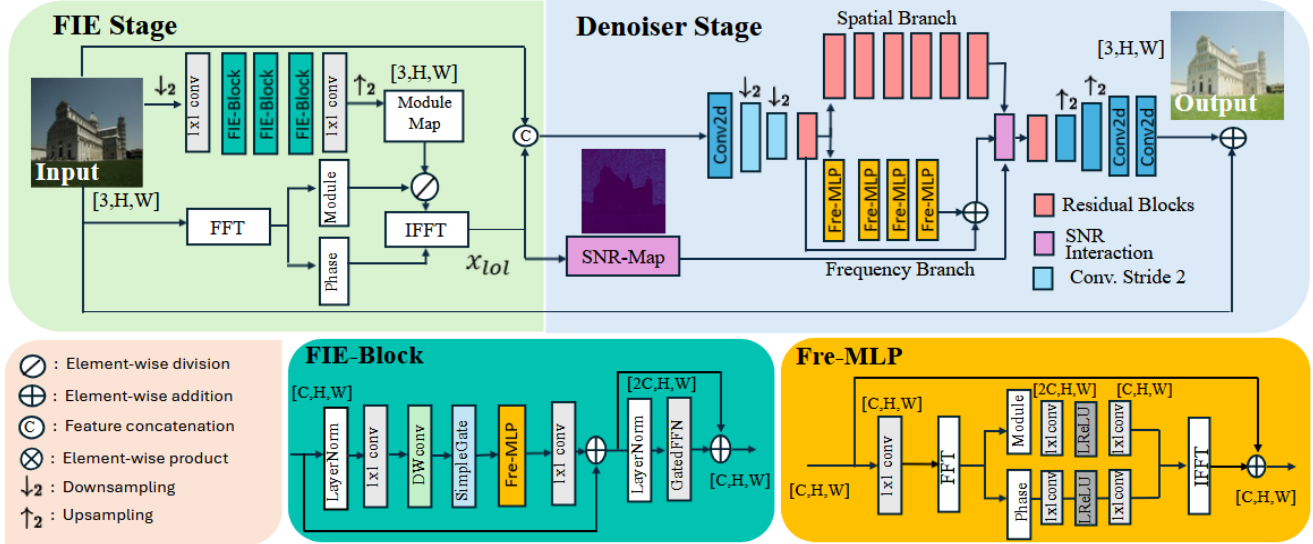


Figure 3. Overview of the proposed model FLOL+. In the first stage, the input image is transformed into the Fourier frequency domain to enhance its illumination level. Next, during the denoiser stage, we correct imperfections such as artifacts and high levels of noise. Note that our model is trained end-to-end.

As result of other Fourier-based procedures [18, 26, 29, 40], we know the following properties in the context of LLIE:

1. The information relative to lightness is contained within the *amplitude* component in the frequency domain.
2. Fourier-based models are capable of extracting *global information* contained in the input image without introducing a huge amount of parameters.

Hence, we design our model in two different steps (please see Fig. 3). The first step, the *Fourier Illumination Enhancement (FIE)* consists on increasing illumination level and retrieving the clear image  $x$  from the dark input  $y$ , by enhancing its amplitude component in the Fourier frequency space. The output from this stage is  $x_{lol}$ , and serves as input of the next stage.

The second step or *Denoiser stage* consists on removing noise, color imperfections and artifacts, by using the Signal-to-Noise-Ratio (SNR) map [51] and emphasizing details recovery. The output will be the reconstructed clean image  $\hat{x}$ .

### 3.1. Fourier Illumination Enhancement (FIE) Stage

In the first place, the input image is converted into its Fourier image using the discrete 2-dimensional Fast Fourier Transform (FFT), and then separated into its phase and module components. Following previous works [26, 40], we focus on enhancing the amplitude component.

To achieve this, we produce the amplitude transform map (or “Module Map”) by feeding the input image into the *FIE-Block*. This block follows a Metaformer [60] structure (also

similar to a NAFBlock [7]):

$$z_1 = \text{Attention}(\text{LayerNorm}(z)) + z \quad (3)$$

$$z_2 = \text{FFN}(\text{LayerNorm}(z_1)) + z_1 \quad (4)$$

where  $z$  are the input features and  $z_2$  the output features of the block. However, we apply global attention in the frequency domain, thanks to the Fourier properties. For this, we design the *Fre-MLP* block that works inside the FIE-Block — a feed-forward network or MLP that operates in the frequency components (please see Fig. 3). We use the same gated FFN (pixel-wise convolutions with simple gates) as NAFNet [7].

Note that we estimate the “Module Map” using a low-resolution input image resized by half ( $\downarrow_2$ ) using bilinear interpolation. This is possible since the amplitude is (partially) scale invariant [26]. Moreover, this allows us to reduce the computation and number of operations notably. The resultant amplitude map is upscaled to the original resolution using the same interpolation.

Finally, we continue by applying the amplitude transform map (“Module Map”) to the original amplitude —via element-wise division— to enhance it. The result is the new amplitude component of the input image, and the non-modified phase. We apply an inverse Fast Fourier Transform (iFFT) to obtain the intermediate result  $x_{lol}$  (please see Fig. 3). This result already presents good illumination properties, but also notable noise and artifacts. In the section ahead, we will explain how to remove this noise and artifacts and how to perform a good color correction. This will allow us to recover the clean image properly.

### 3.2. Denoiser Stage

We focus on improving the previous stage result,  $\mathbf{x}_{lol}$ . We concatenate  $\mathbf{x}_{lol}$  and  $\mathbf{x}$  and feed them into our denoiser.

First, we use an encoder with simple strided  $3 \times 3$  convolutions. Then, we will employ the Fourier space (Frequency branch) and the spatial domain (Spatial branch) along with the SNR map to remove imperfections – see Fig. 3. We calculate the SNR map from the output of the frequency stage in the same way as previous works [40].

The outputs of these branches are  $O_S$  and  $O_F$ , respectively. The SNR-based interaction, shown in Eq. 5, is the combination of  $O_S$  and  $O_F$  with the SNR map ( $R$ ):

$$\mathcal{F} = O_S \times R + O_F \times (1 - R) \quad (5)$$

The output features  $\mathcal{F}$  are fed into the decoder of the Denoiser, together with the encoder skip connections. We use sub-pixel convolutions (Pixel Shuffle) [36] to up-sample the features in the decoder.

Next, we decode the output reconstructed image  $\hat{\mathbf{x}}$  and we apply a global residual connection in which we add to the output image from the decoder the original image (using  $\mathbf{x}$  as a prior). Finally, we obtain the clean image without noise or artifacts and good illumination levels.

### 3.3. Feature Propagation

We discuss the application of concatenation within the decoder structure. We perform skip connections between the encoder and the decoder following the fundamentals of a standard U-net. Those concatenations preserve features across the whole structure and this fact will make the network more efficient as it considers previous information. We can reduce the number of parameters of our network even more by replacing concatenations for feature additions. As a result, the number of channels on each convolutional layer is decreased. For that reason, we will study the performance of this modification in Subsec. 4.4.

### 3.4. Training

We train the models using the following loss function that combines distortion and perception terms:

$$\mathcal{L} = \|\mathbf{x} - \hat{\mathbf{x}}\|_1 + \|\mathbf{x} - \mathbf{x}_{lol}\|_1 + \lambda \cdot \text{LPIPS}(\mathbf{x}, \hat{\mathbf{x}}) \quad (6)$$

The distortion term,  $l_1$  loss, enforces high fidelity. Most importantly, the intermediate loss using  $\mathbf{x}_{lol}$  enforces a good intermediate result *i.e.*, good illumination correction. We use LPIPS [63] (pre-trained VGG-19 [37]) as a perceptual loss, with a weight  $\lambda = 0.1$  found empirically.

## 4. Experimental Results

### 4.1. Datasets and Implementation Details

We train and evaluate our method using well-known datasets for the LLIE problem such as LOLv2-Real [55],

LOLv2-Synthetic [55], LSRW [16], UHD-LL [27], MIT-5K [3] and real scene datasets. It is important to note that LOLv2-Real and LSRW include real-world images captured by using precise camera calibration, for this reason we focus on these, as they represent the most challenging scenarios.

**LOLv2-Real** includes 689 low/high paired images for training and 100 low/high paired images for testing. Note that LOLv2-Real is the extended version of LOL-v1[46], thus, we use the v2 version directly as it is more diverse than LOL-v1. We also use the *LOLv2-Synthetic* that includes 900 pairs of low/high images for training and 100 pairs for validation.

**LSRW** includes images from a DSLM Nikon camera and a Huawei smartphone. The LSRW-Nikon dataset is composed of 3150 training image pairs and 20 testing image pairs. The LSRW-Huawei dataset contains 2450 pairs of images and 30 pairs for training and validation, respectively.

**UHD-LL** includes 2000 pairs of low/high images for training and 150 pairs for validation [27]. All images are in 4K resolution and they are captured using a tripod to ensure stability and to reduce misalignment caused by camera shakes.

**MIT-5k** includes 4500 pairs of low/high images [3]. The images vary in terms of lighting conditions, color balance, and exposure. The ground-truth enhanced images were produced by a professional photographer. We use the same test split of 100 images as SCI [31].

**Unpaired Datasets** such as BDD100k [58] –the driving video dataset–, DICM [24], LIME [15], MEF [30], NPE [42], VV [39] and DarkFace [53] datasets. These datasets offer real low-light scenes in the wild (ground-truth images are not available), we use them for visual evaluation and qualitative assessment.

**Implementation Details.** We train our method using Adam optimizer (with  $\beta_1 = 0.9$  and  $\beta_2 = 0.999$ ) and a learning rate  $4 \times 10^{-4}$  that gradually decreases to  $1 \times 10^{-6}$  using cosine annealing. We use a mini-batch size of 32, considering that we take random crops of size  $256 \times 256$  from the original low/high pair of images. We perform simple augmentations that include flips and rotations. We set to 16 the overall number of channels for each block (or layer) in the network. We use an NVIDIA 4090Ti to train our models in  $\approx 6$  hours.

We train using the LOLv2 [55] and LSRW [16] datasets combined, such that the model can learn from more diverse scenes, sensors and conditions. We evaluate our model using the standard quality metrics PSNR and SSIM [44].

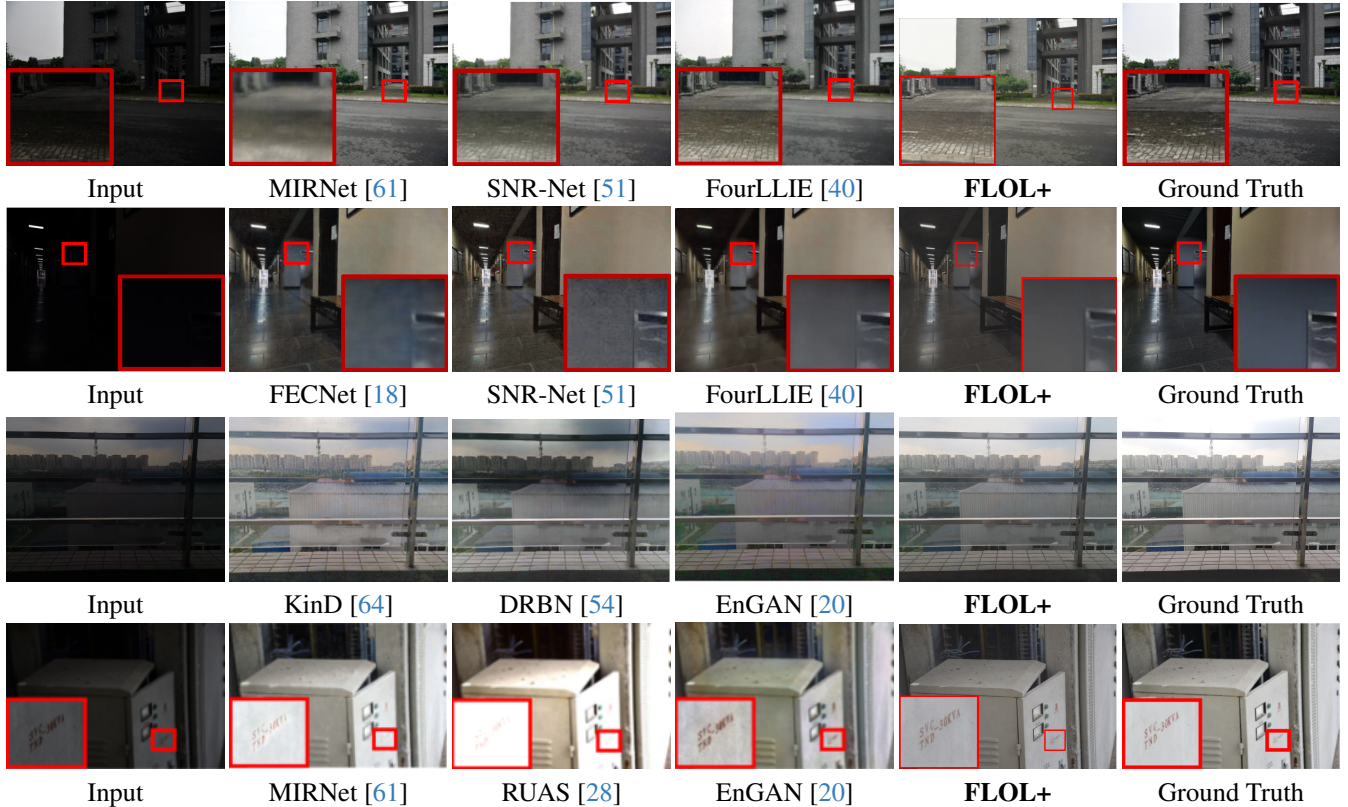


Figure 4. Qualitative results on **LSRW-Nikon** [16] (first and fourth rows) and **LSRW-Huawei** [16] (second and third rows).

Table 1. Quantitative comparison of the retrained state of the arts on the **UHD-LL** dataset [27]. The best result is in **red** color, second best in **blue**. All the values are adopted from [27].

	Uformer [45]	SNR-Net(r) [51]	SNR-Net(s) [51]	UHDFour [27]	Restormer(s) [62]
PSNR $\uparrow$	19.283	22.717	22.170	<b>26.226</b>	22.252
SSIM $\uparrow$	0.849	0.877	0.866	<b>0.900</b>	0.871
	Restormer [62]	ZDCE [14]	RUAS [28]	SCI [31]	<b>FLOL+ (Ours)</b>
PSNR $\uparrow$	22.597	17.075	13.562	16.057	<b>25.01</b>
SSIM $\uparrow$	0.878	0.663	0.749	0.625	<b>0.888</b>

## 4.2. Comparison with Other Methods

**Quantitative Results.** We present our model performance on several datasets, UHD-LL, LSRW and MIT-5k, in Tabs. 1, 2 and 3, respectively. In addition, we show our model performance compared with a wide range of SOTA models in Tab. 4 and Fig. 1. Also in Tab. 5, we calculate a perceptual metric of quality assessment called BRISQUE [32] in our qualitative results and we compare them with other SOTA methods again. Our solution accomplishes good results if we compare with other procedures like SNR-Net [51] or MIRNet [61]. In particular, our

model requires  $37\times$  and almost  $300\times$  less parameters, respectively, to reach similar or better performance. Compared to the most recent method, Retinexformer [4], our model gets a comparable performance with  $10\times$  **fewer parameters**, and  $7\times$  **less FLOPs**. Also, our procedure outperforms FourLLIE [40], the best previous method in terms of efficiency-performance trade-off, by **+0.6 dB** in the LOLv2-Real. Note, that we report quantitative results for some methods based on previous analysis [4], and we use the open-source weights and models of FourLLIE [40].

Our method FLOL+ outperforms in terms of image quality and/or efficiency all the previous methods.

**Qualitative Results.** The visual comparison between our algorithm and other SOTA methods on real scenes is shown in Figs. 4, 5, 8 and 11, corresponding to paired datasets. Our method produces high-quality results with good color correction and details, without adding noise or artifacts to the image, and effectively increases the “light” and brightness of the image, improving its visibility as a result. To prove the robustness of our approach, we also apply our model to random real scenes from unpaired datasets like BDD100k [58], DICM [24], LIME [15], MEF [30], NPE [42], VV [39] and DarkFace [53]. The results are

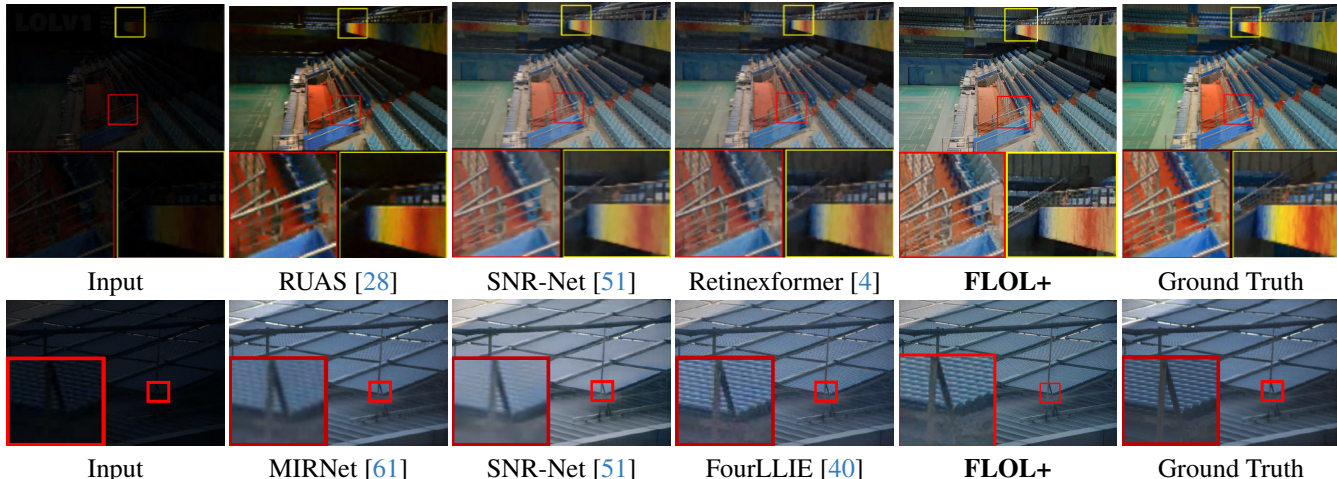


Figure 5. Qualitative results on **LOLv1** [46] (first row) and **LOLv2-Real** [55] (second row) datasets.

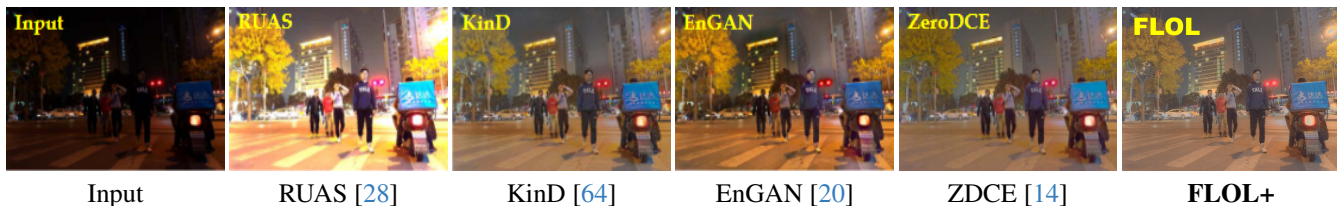


Figure 6. Qualitative results on **DarkFace** [53] dataset.

Table 2. Quantitative comparisons on the **LSRW** dataset (50 test images from Huawei and Nikon) [16]. Our method achieves the best results in terms of fidelity and perceptual metrics. Reference values are adopted from [31, 52].

	RetinexNet [46]	FIDE [48]	DRBN [54]	KinD [64]	STAR [47]
PSNR $\uparrow$	15.906	<b>17.669</b>	16.149	16.472	14.608
SSIM $\uparrow$	0.3725	<b>0.5485</b>	0.5422	0.4929	0.5039
LPIPS $\downarrow$	0.393	-	0.376	-	-
	EnGAN [20]	ZDCE [14]	RUAS [28]	SCI [31]	<b>FLOL+</b> <b>(Ours)</b>
PSNR $\uparrow$	16.311	15.834	14.437	15.017	<b>19.10</b>
SSIM $\uparrow$	0.4697	0.4664	0.4276	0.4846	<b>0.5833</b>
LPIPS $\downarrow$	0.322	<b>0.315</b>	0.455	0.321	<b>0.273</b>

shown in Figs. 6, 7, 9 and 10. Our model is robust and can generalize on these unseen and challenging datasets. We can observe a significant improvement after applying our method.

### 4.3. Efficiency and Runtime

We conduct a runtime experiment in which we have chosen a sample video from BDD100k [58] dataset. We selected

Table 3. Quantitative comparisons on the **MIT-5K** dataset [2]. All the values are adopted from [31].

	RetinexNet [46]	FIDE [48]	DRBN [54]	KinD [64]	STAR [47]
PSNR $\uparrow$	13.74	17.19	17.59	17.09	17.64
SSIM $\uparrow$	0.739	0.785	0.784	0.830	0.779
	EnGAN [20]	ZDCE [14]	RUAS [28]	SCI [31]	<b>FLOL+</b> <b>(Ours)</b>
PSNR $\uparrow$	16.76	16.61	18.53	<b>20.44</b>	<b>22.10</b>
SSIM $\uparrow$	0.834	0.814	0.864	<b>0.893</b>	<b>0.910</b>

some frames by cropping the video sample and we changed the spatial resolution several times to calculate the processing runtime rate when we apply our method. To demonstrate the efficiency of our solution, we measure the number of operations (FLOPs) and runtime at those different resolutions. In Tab. 6 we provide the study and comparison with FourLLIE [40], one of the fastest solutions. We measure runtimes 1000 times per frame, and we report the average runtime. Our method has notably less parameters and FLOPs than previous state-of-the-art methods, which translates into real-time performance. We can process full-

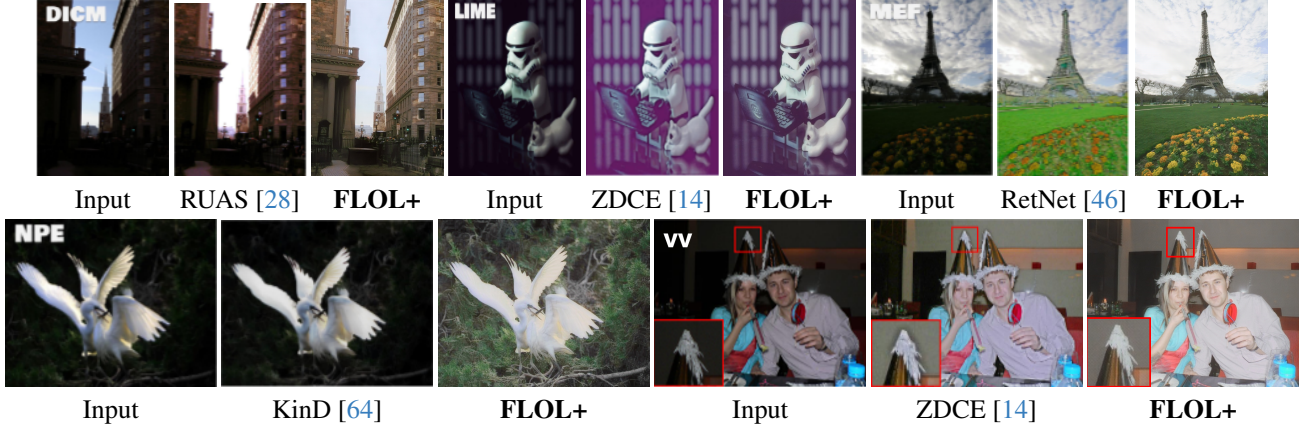


Figure 7. Qualitative results on **DICM** [24], **LIME** [15], **MEF** [30], **NPE** [42] and **VV** [39].

Table 4. Quantitative comparisons on the **LOLv2** dataset [55]. Our model obtains a comparable performance with the best SOTA methods, while being notably smaller (less parameters and operations) and more efficient. All values are collected from [4, 40]. FLOPs were calculated using input image of size  $256 \times 256$ .

Methods	Complexity		LOLv2-Real		LOLv2-Syn	
	FLOPs (G) $\downarrow$	Params (M) $\downarrow$	PSNR $\uparrow$	SSIM $\uparrow$	PSNR $\uparrow$	SSIM $\uparrow$
SID [5]	13.73	7.76	13.24	0.442	15.04	0.610
DeepUPE [41]	21.10	1.02	13.27	0.452	15.08	0.623
RF [22]	46.23	21.54	14.05	0.458	15.97	0.632
DeepLPE [33]	5.86	1.77	14.10	0.480	16.02	0.587
IPF [6]	6887	115.31	19.80	0.813	18.30	0.811
UFormer [45]	12.00	5.29	18.82	0.771	19.66	0.871
RetinexNet [46]	587.47	0.84	15.47	0.567	17.13	0.798
Sparse [55]	53.26	2.33	20.06	0.816	22.05	0.905
EnGAN [20]	61.01	114.35	18.23	0.617	16.57	0.734
RUAS [28]	<b>0.83</b>	<b>0.003</b>	18.37	0.723	16.55	0.652
FIDE [48]	28.51	8.62	16.85	0.678	15.20	0.612
DRBN [54]	48.61	5.27	20.29	0.831	23.22	0.927
KinD [64]	34.99	8.02	14.74	0.641	13.29	0.578
Restormer [62]	144.25	26.13	19.94	0.827	21.41	0.830
FECNet [18]	11.84	0.15	20.67	0.795	22.57	0.893
MIRNet [61]	785	31.76	20.02	0.820	21.94	0.876
SNR-Net [51]	26.35	4.01	21.48	0.849	24.14	<b>0.928</b>
FourLLIE [40]	5.8	0.120	21.60	<b>0.847</b>	24.17	0.917
Retinexformer [4]	15.57	1.61	22.80	0.840	<b>25.67</b>	<b>0.930</b>
<b>FLOL+ (Ours)</b>	<b>2.08</b>	<b>0.094</b>	<b>21.75</b>	<b>0.849</b>	<b>24.34</b>	<b>0.906</b>
<b>FLOL (Ours)</b>	8.36	0.806	<b>23.06</b>	0.837	-	-

Table 5. Quantitative comparison on five unpaired datasets using the blind quality assessment metric BRISQUE [32].

Methods	<b>DICM</b>	<b>LIME</b>	<b>MEF</b>	<b>NPE</b>	<b>VV</b>
KinD [64]	48.72	39.91	49.94	36.85	50.56
RUAS [28]	38.75	27.59	<b>23.68</b>	47.85	38.37
LLFlow [43]	<b>26.36</b>	<b>27.06</b>	30.27	28.86	<b>31.67</b>
SNR-Net [51]	37.35	39.22	31.28	<b>26.65</b>	78.72
PairLIE [12]	33.31	<b>25.23</b>	<b>27.53</b>	28.27	39.13
<b>FLOL+ (Ours)</b>	<b>30.36</b>	<b>28.65</b>	<b>33.79</b>	<b>16.79</b>	<b>19.97</b>

HD images at  $> 60$  FPS on consumer GPUs. Considering the low memory requirements, the model could be also

used in mobile devices. We also apply the detection model YOLOv8 [35] before and after of processing those frames with FLOL+. The qualitative results are shown in Fig. 9, where we can see the remarkable improvement in the detection task. In conclusion, our method gets similar results, considering its features and limitations, when compared with other methods which have been used on mobile phones [9] with different capabilities.

#### 4.4. Ablation Study

In Tab. 7 we compare efficiency and performance depending on how we propagate the features from the denoiser encoder to the decoder. Concatenation allows to accumulate more information at the expense of efficiency. When the number of channels is high (64), the denoiser can produce rich features, and simply adding the encoder-decoder skip connections works optimally. We call FLOL+ to the fastest version of our model.

#### 4.5. Limitations

As we show in Figs. 9 and 10, our model sometimes struggles on low-light images from unknown sensors. However, training our model using more diverse data –captured from multiple sensors– will lead to better generalization.

### 5. Conclusion

We focus on solving the low-light image enhancement (LLIE) problem from the efficiency and robustness point of view. We present a new method called FLOL+, and end-to-end neural network with two main blocks: FIE enhancement and a denoiser. Our method achieves state-of-the-art results in real-world low-light benchmarks. Moreover, it requires  $10\times$  less parameters, and has  $7\times$  less FLOPs operations than previous works. This allows us to process HD images in real-time. In addition, FLOL+, represents a new baseline with a notable robustness in real scenarios.

Table 6. **Efficiency Ablation Study.** We report the FLOPs and runtime of our model at different image resolutions. Runtimes are calculated using a NVIDIA GeForce RTX 4090. Note that Retinexformer [4] fails (OOM) with high resolution images.

Spatial Resolution (px)	FLOPs (G) ↓			Runtime (ms) ↓		
	Retinexformer [4]	FourLLIE [40]	<b>FLOL+</b>	Retinexformer [4]	FourLLIE [40]	<b>FLOL+</b>
640 × 480	160.4	24.46	<b>9.7</b>	55.2	6.8	<b>3.4</b>
1280 × 720	481.2	73.38	<b>39.12</b>	176.8	20.9	<b>5.4</b>
1920 × 1080	OOM	165.08	<b>65.52</b>	409.6	64.9	<b>12.4</b>
2560 × 1440	OOM	293.48	<b>116.46</b>	751.3	123.9	<b>24.2</b>

Table 7. **Architecture Ablation Study.** We compare two strategies to propagate features from encoder to decoder. NC stands for “number of channels” of the convolutional layers. We define **FLOL** as the most complex model, and **FLOL+** as the fastest variant.

NC	Feature Concatenation				Feature Addition			
	PSNR↑	SSIM↑	Parameters (M)↓	FLOPs (G)↓	PSNR↑	SSIM↑	Parameters (M)↓	FLOPs (G)↓
16	21.75	0.849	0.094	2.08	21.13	0.813	0.055	0.736
32	22.33	0.833	0.364	7.62	22.64	0.823	0.206	2.34
64	22.02	0.817	1.44	29.48	23.06	0.837	0.806	8.36

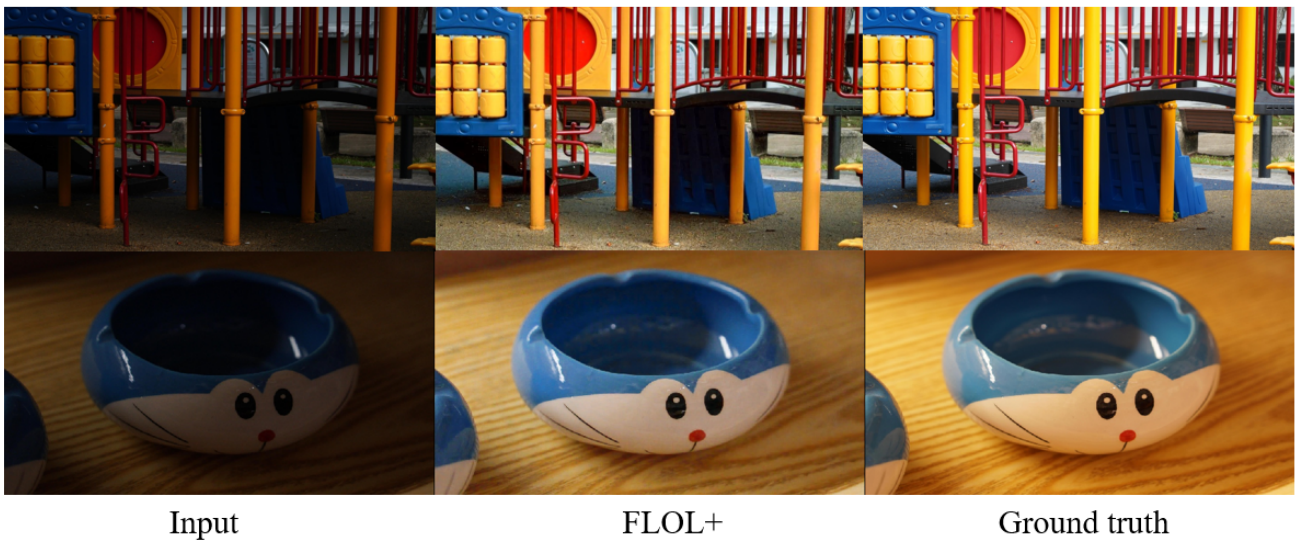


Figure 8. UHD Qualitative results using FLOL+ on the **UHD-LL** [27] real dataset.

## Acknowledgements

The authors thank Supercomputing of Castile and Leon (SCAYLE, Leon, Spain) for assistance with the model training and GPU resources.

This work was supported by Spanish funds through Regional Funding Agency Institute for Business Competitiveness of Castile and Leon (MACS.2 project “Investigación en tecnologías del ámbito de la movilidad autónoma, conectada, segura y sostenible”).

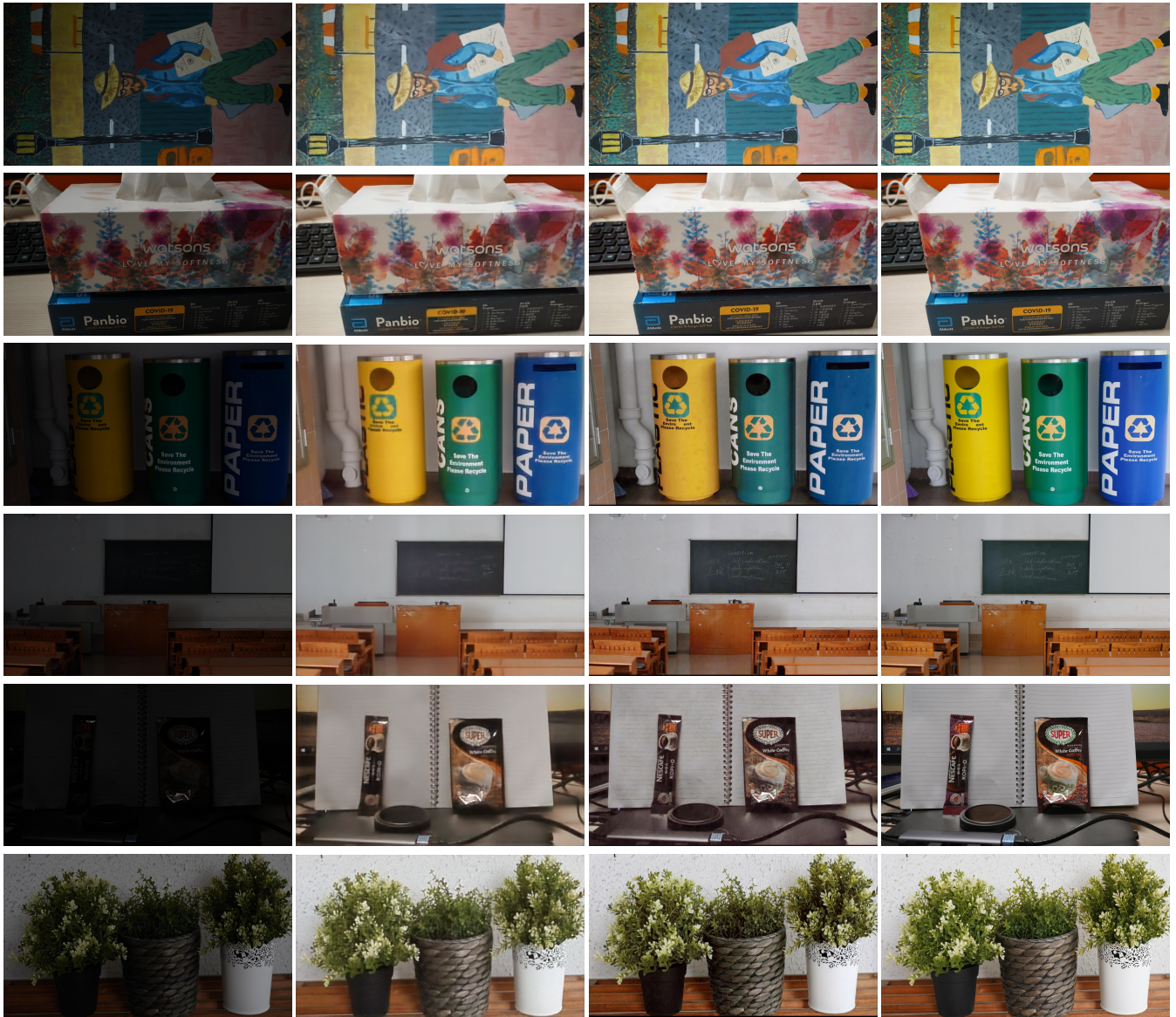




Figure 9. Results of FLOL+ in a sequence of frames belonging to a video from the **BDD100k** [58] dataset. We run again YOLOv8 in both images (low and high), where green labels correspond to class truck and orange labels correspond to class car. (Zoom in for best view).



Figure 10. Comparison of qualitative results on the Autonomous Driving Dataset **BDD100k** [58]. We can observe how the detector YOLOv8 [35] performs best when we use our method for image enhancement.



Input

UHDFour [27]

FLOL+

Ground Truth

Figure 11. Qualitative results on UHD-LL high resolution dataset [27] with images of  $3840 \times 2160$ . (Zoom in for best view).

## References

- [1] Abdelrahman Abdelhamed, Stephen Lin, and Michael S Brown. A high-quality denoising dataset for smartphone cameras. In *CVPR*, pages 1692–1700, 2018. 1
- [2] Vladimir Bychkovsky, Sylvain Paris, Eric Chan, and Frédo Durand. Learning photographic global tonal adjustment with a database of input/output image pairs. In *CVPR*, 2011. 6
- [3] Vladimir Bychkovsky, Sylvain Paris, Eric Chan, and Frédo Durand. Learning photographic global tonal adjustment with a database of input / output image pairs. In *The Twenty-Fourth IEEE Conference on Computer Vision and Pattern Recognition*, 2011. 4
- [4] Yuanhao Cai, Hao Bian, Jing Lin, Haoqian Wang, Radu Timofte, and Yulun Zhang. Retinexformer: One-stage retinex-based transformer for low-light image enhancement. In *Proceedings of the IEEE/CVF International Conference on Computer Vision (ICCV)*, pages 12504–12513, 2023. 1, 2, 5, 6, 7, 8, 9
- [5] Chen Chen, Qifeng Chen, Minh N Do, and Vladlen Koltun. Seeing motion in the dark. In *ICCV*, 2019. 7
- [6] Han ting Chen, Yunhe Wang, Tianyu Guo, Chang Xu, Yiping Deng, Zhenhua Liu, Siwei Ma, Chunjing Xu, Chao Xu, and Wen Gao. Pre-trained image processing transformer. In *CVPR*, 2021. 7
- [7] Liangyu Chen, Xiaojie Chu, Xiangyu Zhang, and Jian Sun. Simple baselines for image restoration. In *European conference on computer vision*, pages 17–33. Springer, 2022. 3
- [8] Sunghyun Cho, Jue Wang, Seungyong Lee, b, and c. Video deblurring for hand-held cameras using patch-based synthesis. In *ACM TOG*, 2012. 1
- [9] Marcos V. Conde, F. Vasluianu, J. Vazquez-Corral, and R. Timofte. Perceptual image enhancement for smartphone real-time applications. In *Proceedings of the IEEE/CVF Winter Conference on Applications of Computer Vision*, 2023. 7
- [10] Michael Elad and Arie Feuer. Restoration of a single super-resolution image from several blurred, noisy, and undersampled measured images. *IEEE Transactions on Image Processing*, 6(12):1646–1658, 1997. 1
- [11] Xueyang Fu, Delu Zeng, Yue Huang, Yinghao Liao, Xinghao Ding, and John Paisley. A fusion-based enhancing method for weakly illuminated images. *Signal Processing*, 2016. 1
- [12] Zhenqi Fu, Yan Yang, Xiaotong Tu, Yue Huang, Xinghao Ding, and Kai-Kuang Ma. Learning a simple low-light image enhancer from paired low-light instances. In *Proceedings of the IEEE/CVF Conference on Computer Vision and Pattern Recognition*, pages 22252–22261, 2023. 7
- [13] Dario Fuoli, Luc Van Gool, and Radu Timofte. Fourier space losses for efficient perceptual image super-resolution. In *IEEE Conf. Computer Vis. Pattern Recog.*, pages 2360–2369, 2021. 2
- [14] Chunle Guo, Chongyi Li, Jichang Guo, Chen Change Loy, Junhui Hou, Sam Kwong, and Runmin Cong. Zero-reference deep curve estimation for low-light image enhancement. In *CVPR*, 2020. 2, 5, 6, 7
- [15] Xiaojie Guo, Yu Li, and Haibin Ling. Lime: Low-light image enhancement via illumination map estimation. *TIP*, 2016. 4, 5, 7
- [16] Jiang Hai, Zhu Xuan, Ren Yang, Yutong Hao, Fengzhu Zou, Fang Lin, and Songchen Han. R2rnet: Low-light image enhancement via real-low to real-normal network. *Journal of Visual Communication and Image Representation*, 90: 103712, 2023. 4, 5, 6
- [17] Samuel W Hasinoff. Photon, poisson noise. *Computer Vision, A Reference Guide*, 4, 2014. 1
- [18] Jie Huang, Yajing Liu, Feng Zhao, and Keyu Yan. Deep fourier-based exposure correction with spatial-frequency interaction. In *Computer Vision-ECCV 2022*, pages 163–180, 2022. 2, 3, 5, 7
- [19] Xingyu Jiang, Xiuhui Zhang, Ning Gao, and Yue Deng. When fast fourier transform meets transformer for image restoration. 2
- [20] Yifan Jiang, Xinyu Gong, Ding Liu, Yu Cheng, Chen Fang, Xiaohui Shen, Jianchao Yang, Pan Zhou, and Zhangyang Wang. Enlightengan: Deep light enhancement without paired supervision. *TIP*, 2021. 5, 6, 7
- [21] Daniel J Jobson, Zia-ur Rahman, and Glenn A Woodell. A multiscale retinex for bridging the gap between color images and the human observation of scenes. *TIP*, 1997. 1
- [22] Satoshi Kosugi and Toshihiko Yamasaki. Unpaired image enhancement featuring reinforcement-learning-controlled image editing software. In *AAAI*, 2020. 7
- [23] Edwin H Land. The retinex theory of color vision. *Scientific american*, 1977. 1
- [24] Chulwoo Lee, Chul Lee, and Chang-Su Kim. Contrast enhancement based on layered difference representation of 2d histograms. *IEEE Transactions on Image Processing*, 22(12):5372–5384, 2013. 4, 5, 7
- [25] Chongyi Li, Chunle Guo, Linghao Han, and Jun Jiang. Low-light image and video enhancement using deep learning: A survey. In *IEEE Trans. Pattern Anal. Mach. Intell.* 44, 12, pages 9396–9416, 2021. 1
- [26] Chongyi Li, Chun-Le Guo, Man Zhou, Zhixin Liang, Shangchen Zhou, Ruicheng Feng, and Chen Change Loy. Embedding fourier for ultra-high-definition low-light image enhancement. In *ICLR*, 2023. 2, 3
- [27] Chongyi Li, Chun-Le Guo, Man Zhou, Zhixin Liang, Shangchen Zhou, Ruicheng Feng, and Chen Change Loy. Embedding fourier for ultra-high-definition low-light image enhancement. In *ICLR*, 2023. 2, 4, 5, 8, 9, 10
- [28] Risheng Liu, Long Ma, Jiaao Zhang, Xin Fan, and Zhongxuan Luo. Retinex-inspired unrolling with cooperative prior architecture search for low-light image enhancement. In *CVPR*, 2021. 5, 6, 7
- [29] Xiaoqian Lv, Shengping Zhang, Chenyang Wang, Yichen Zheng, Bineng Zhong, Chongyi Li, and Liqiang Nie. Fourier priors-guided diffusion for zero-shot joint low-light enhancement and deblurring. In *Proceedings of the IEEE/CVF Conference on Computer Vision and Pattern Recognition*, pages 25378–25388, 2024. 3
- [30] Kede Ma, Kai Zeng, and Zhou Wang. Perceptual quality assessment for multi-exposure image fusion. *TIP*, 2015. 4, 5, 7
- [31] Long Ma, Tengyu Ma, Risheng Liu, Xin Fan, and Zhongxuan Luo. Toward fast, flexible, and robust low-light image enhancement. In *CVPR*, 2022. 1, 2, 4, 5, 6

- [32] Anish Mittal, Anush Krishna Moorthy, and Alan Conrad Bovik. No-reference image quality assessment in the spatial domain. *IEEE Transactions on Image Processing*, 21(12):4695–4708, 2012. 5, 7
- [33] Sean Moran, Pierre Marza, Steven McDonagh, Sarah Parisot, and Gregory Slabaugh. Deeplpf: Deep local parametric filters for image enhancement. In *CVPR*, 2020. 7
- [34] Emmanuel Onzon, Fahim Mannan, and Felix Heide. Neural auto-exposure for high-dynamic range object detection. In *Proceedings of the IEEE/CVF conference on computer vision and pattern recognition*, pages 7710–7720, 2021. 1
- [35] Joseph Redmon, Ali Farhadi, Santosh Divvala, and Ross Girshick. You only look once: Unified, real-time object detection. *arXiv preprint arXiv:1506.02640*, 2015. 7, 9
- [36] Wenzhe Shi, Jose Caballero, Ferenc Huszár, Johannes Totz, Andrew P Aitken, Rob Bishop, Daniel Rueckert, and Zehan Wang. Real-time single image and video super-resolution using an efficient sub-pixel convolutional neural network. In *Proceedings of the IEEE conference on computer vision and pattern recognition*, pages 1874–1883, 2016. 4
- [37] K Simonyan and A. Zisserman. Very deep convolutional networks for large-scale image recognition. *arXiv preprint arXiv:1409.1556*, 2014. 4
- [38] Ashish Vaswani, Noam Shazeer, Niki Parmar, Jakob Uszkoreit, Llion Jones, Aidan N Gomez, Łukasz Kaiser, and Illia Polosukhin. Attention is all you need. *Advances in neural information processing systems*, 30, 2017. 2
- [39] Vassilios Vonikakis, Rigas Kouskouridas, and Antonios Gasteratos. On the evaluation of illumination compensation algorithms. *Multimedia Tools and Applications*, 2018. 4, 5, 7
- [40] Chenxi Wang, Hongjun Wu, and Zhi Jin. Fourllie: Boosting low-light image enhancement by fourier frequency information. In *Proceedings of the 31st ACM International Conference on Multimedia*, pages 7459–7469, 2023. 1, 2, 3, 4, 5, 6, 7, 8
- [41] Ruixing Wang, Qing Zhang, Chi-Wing Fu, Xiaoyong Shen, Wei-Shi Zheng, and Jiaya Jia. Underexposed photo enhancement using deep illumination estimation. In *CVPR*, 2019. 7
- [42] Shuhang Wang, Jin Zheng, Hai-Miao Hu, and Bo Li. Naturalness preserved enhancement algorithm for non-uniform illumination images. *IEEE Transactions on Image Processing*, 22(9):3538–3548, 2013. 4, 5, 7
- [43] Yufei Wang, Renjie Wan, Wenhan Yang, Haoliang Li, Lap-Pui Chau, and Alex C Kot. Low-light image enhancement with normalizing flow. *arXiv preprint arXiv:2109.05923*, 2021. 7
- [44] Zhou Wang, Alan C Bovik, Hamid R Sheikh, and Eero P Simoncelli. Image quality assessment: from error visibility to structural similarity. *TIP*, 2004. 1, 4
- [45] Zhendong Wang, Xiaodong Cun, Jianmin Bao, and Jianzhuang Liu. Uformer: A general u-shaped transformer for image restoration. In *CVPR*, 2022. 5, 7
- [46] Chen Wei, Wenjing Wang, Wenhan Yang, and Jiaying Liu. Deep retinex decomposition for low-light enhancement. In *BMVC*, 2018. 1, 2, 4, 6, 7
- [47] Jun Xu, Yingkun Hou, Dongwei Ren, Li Liu, Fan Zhu, Mengyang Yu, Haoqian Wang, and Ling Shao. Star: A structure and texture aware retinex model. *IEEE Transactions on Image Processing*, 29:5022–5037, 2020. 6
- [48] Ke Xu, Xin Yang, Baocai Yin, and Rynson WH Lau. Learning to restore low-light images via decomposition-and-enhancement. In *CVPR*, 2020. 6, 7
- [49] Qinwei Xu, Ruipeng Zhang, Ya Zhang, Yanfeng Wang, and Qi Tian. A fourier-based framework for domain generalization. In *IEEE*, 2021. 2
- [50] Ruikang Xu, Chang Chen, Jingyang Peng, Cheng Li, Yibin Huang, Fenglong Song, Youliang Yan, and Zhiwei Xiong. Toward raw object detection: A new benchmark and a new model. In *Proceedings of the IEEE/CVF Conference on Computer Vision and Pattern Recognition*, pages 13384–13393, 2023. 1
- [51] Xiaogang Xu, Ruixing Wang, Chi-Wing Fu, and Jiaya Jia. Snr-aware low-light image enhancement. In *CVPR*, 2022. 2, 3, 5, 6, 7, 9
- [52] Shuzhou Yang, Moxuan Ding, Yanmin Wu, Zihan Li, and Jian Zhang. Implicit neural representation for cooperative low-light image enhancement. In *Proceedings of the IEEE/CVF International Conference on Computer Vision (ICCV)*, pages 12918–12927, 2023. 6
- [53] Wenhan Yang, Ye Yuan, Wenqi Ren, Jiaying Liu, Walter J. Scheirer, Zhangyang Wang, Taiheng Zhang, Qiaoyong Zhong, Di Xie, Shiliang Pu, Yuqiang Zheng, Yanyun Qu, Yuhong Xie, Liang Chen, Zhonghao Li, Chen Hong, Hao Jiang, Siyuan Yang, Yan Liu, Xiaochao Qu, Pengfei Wan, Shuai Zheng, Minhui Zhong, Taiyi Su, Lingzhi He, Yandong Guo, Yao Zhao, Zhenfeng Zhu, Jinxiu Liang, Jingwen Wang, Tianyi Chen, Yuhui Quan, Yong Xu, Bo Liu, Xin Liu, Qi Sun, Tingyu Lin, Xiaochuan Li, Feng Lu, Lin Gu, Shengdi Zhou, Cong Cao, Shifeng Zhang, Cheng Chi, Chubing Zhuang, Zhen Lei, Stan Z. Li, Shizheng Wang, Ruizhe Liu, Dong Yi, Zheming Zuo, Jianning Chi, Huan Wang, Kai Wang, Yixiu Liu, Xingyu Gao, Zhenyu Chen, Chang Guo, Yongzhou Li, Huicai Zhong, Jing Huang, Heng Guo, Jianfei Yang, Wenjuan Liao, Jiangang Yang, Liguozhou, Mingyue Feng, and Likun Qin. Advancing image understanding in poor visibility environments: A collective benchmark study. *IEEE Transactions on Image Processing*, 29:5737–5752, 2020. 4, 5, 6
- [54] Wenhan Yang, Shiqi Wang, Yuming Fang, Yue Wang, and Jiaying Liu. Band representation-based semi-supervised low-light image enhancement: Bridging the gap between signal fidelity and perceptual quality. *TIP*, 2021. 5, 6, 7
- [55] Wenhan Yang, Wenjing Wang, Haofeng Huang, Shiqi Wang, and Jiaying Liu. Sparse gradient regularized deep retinex network for robust low-light image enhancement. *TIP*, 2021. 1, 4, 6, 7
- [56] Masakazu Yoshimura, Junji Otsuka, Atsushi Irie, and Takeshi Ohashi. Dynamicisp: dynamically controlled image signal processor for image recognition. In *Proceedings of the IEEE/CVF International Conference on Computer Vision*, pages 12866–12876, 2023. 1
- [57] Masakazu Yoshimura, Junji Otsuka, Atsushi Irie, and Takeshi Ohashi. Rawgment: Noise-accounted raw augmen-

tation enables recognition in a wide variety of environments. In *Proceedings of the IEEE/CVF Conference on Computer Vision and Pattern Recognition*, pages 14007–14017, 2023. 1

- [58] Fisher Yu, Haofeng Chen, Xin Wang, Wenqi Xian, Yingying Chen, Fangchen Liu, Vashisht Madhavan, and Trevor Darrell. Bdd100k: A diverse driving dataset for heterogeneous multitask learning. In *IEEE/CVF Conference on Computer Vision and Pattern Recognition (CVPR)*, 2020. 4, 5, 6, 9
- [59] Hu Yu, Naishan Zheng, Man Zhou, Jie Huang, Xiao Zeyu, and Feng Zhao. Frequency and spatial dual guidance for image dehazing. In *ECCV*, 2022. 2
- [60] Weihao Yu, Mi Luo, Pan Zhou, Chenyang Si, Yichen Zhou, Xinchao Wang, Jiashi Feng, and Shuicheng Yan. Metaformer is actually what you need for vision. In *Proceedings of the IEEE/CVF conference on computer vision and pattern recognition*, pages 10819–10829, 2022. 3
- [61] Syed Waqas Zamir, Aditya Arora, Salman Khan, Munawar Hayat, Fahad Shahbaz Khan, Ming-Hsuan Yang, and Ling Shao. Learning enriched features for real image restoration and enhancement. In *ECCV*, 2020. 5, 6, 7
- [62] Syed Waqas Zamir, Aditya Arora, Salman Khan, Munawar Hayat, Fahad Shahbaz Khan, and Ming-Hsuan Yang. Restormer: Efficient transformer for high-resolution image restoration. In *CVPR*, 2022. 5, 7
- [63] Richard Zhang, Phillip Isola, Alexei A Efros, Eli Shechtman, and Oliver Wang. The unreasonable effectiveness of deep features as a perceptual metric. In *CVPR*, 2018. 4
- [64] Yonghua Zhang, Jiawan Zhang, and Xiaojie Guo. Kindling the darkness: A practical low-light image enhancer. In *ACM MM*, 2019. 1, 5, 6, 7
- [65] Man Zhou, Jie Huang, Chongyi Li, Hu Yu, Keyu Yan, Naishan Zheng, and Feng Zhao. Adaptively learning low-high frequency information integration for pan-sharpening. In *ACM*, 2022. 2
- [66] Man Zhou, Jie Huang, Keyu Yan, Hu Yu, Fu Xueyang, Aiping Liu, Xian Wei, and Feng Zhao. Spatial-frequency domain information integration for pan-sharpening. In *ECCV*, 2022. 2
- [67] Man Zhou, Hu Yu, Jie Huang, Feng Zhao, Jinwei Gu, Chen Change Loy, Deyu Meng, and Chongyi Li. Deep fourier up-sampling. In *Adv. Neural Inform*, 2022. 2